https://doi.org/10.3311/PPtr.41231
Creative Commons Attribution

Periodica Polytechnica Transportation Engineering

Aerodynamic Design and CFD-based Performance Analysis of UAV Wing Ailerons

Agus Suprianto[1*], Dede Santoso[1], Singgih Satrio Wibowo[2], Arif Krisbudiman[1,3], Mohamad Dahsyat[1], Rismu Landung Gumilang[1], Fadjar Rahino Triputra[1], Jimmy Maulana[1], Suherman Mukti[1]

[1] National Research and Innovation Agency, Jl. Raya Puspiptek 60, Setu, South Tangerang, Banten, 15314, Indonesia
[2] Bandung State Polytechnic, Jl. Ciwaruga, Ciwaruga, Kec. Parongpong, Kabupaten, West Bandung, Jawa Barat, 40559, Indonesia
[3] Indonesian Institute of Technology, Jl. Puspitek, Setu, Kec. Serpong, Kota, South Tangerang, Banten, 15314, Indonesia
[*] Corresponding author, e-mail: agus137@brin.go.id

Received: 10 June 2025, Accepted: 15 March 2026, Published online: 10 November 2026

Abstract

The aerodynamic efficiency of wing control surfaces is critical in optimizing aircraft performance. This study focuses on the aerodynamic design of ailerons adhering to military standards (MIL-STD-1797) to enhance their efficiency using hybrid analytical-empirical approach. Computational Fluid Dynamics (CFD)-based analyses of flow characteristics, aerodynamic forces, and efficiency were conducted to identify optimal aileron configurations. Variations in deflection angles were evaluated based on aircraft classes, flight phases, acceptance criteria, inboard and outboard positions, and wing effectiveness. The SST k-omega turbulence model was selected to improve accuracy in predicting transitional flows around the aileron. Results indicate that the optimal configuration includes an aileron length of 26.1% of the wingspan, a width of 20% of the wing chord, and a maximum deflection angle of 20 degrees with the Cl/Cd value is approximately 3.92. Also, the optimal position at 68.9% of the wing inboard, and 95% of the wing outboard.

Keywords

aileron efficiency, aerodynamic design, computational fluid dynamics

1 Introduction

A review of aerodynamic efficiency in the field of flight control represents a fundamental component in the design of modern aircraft. The aileron is a crucial element within the lateral control system of the aircraft, serving to facilitate roll maneuvers and maintain stability during flight (Brincklow and Hunsaker, 2020, Brincklow and Hunsaker, 2021; Brincklow et al., 2024).

In military aircraft design, the performance of the aileron must comply with stringent requirements as outlined in MIL-STD-1797 (US Deptartment of Defense, 1995) standards to ensure flight quality based on precise control design (Wang and Zhou, 2025). This includes meeting operational demands under various flight conditions, such as high-speed scenarios, extreme maneuvers, and turbulent environments (Dong et al., 2024; Takahashi et al., 2025). This standard establishes performance limitations encompassing control effectiveness, static and dynamic stability, as well as their impact on the aerodynamic load distribution of the wings. It applies to various types of aircraft that may differ significantly in weight and operational altitude yet possess similar maneuvering capabilities and fulfill identical mission requirements.

The study of aileron efficiency has become increasingly relevant with the growing demand for unmanned aerial vehicles capable of performing highly responsive maneuvers without significantly increasing drag. In this context, Susilo, et al. (2024) have explored the application of electromechanical systems in aircraft aileron control, representing a step toward the development of More Electric Aircraft (MEA) and Zero Emission Aircraft (ZEA). Furthermore, Negahban, et al. (2024) designed the aileron using morphing technology with the Free Form Deformation (FFD) concept to enhance control and flight performance. Subsequently, Arifin and Subchan (2017) conducted research on the effectiveness of deflection angles in the optimization of aileron control surfaces through experimental investigations. Besides that, Brincklow and Hunsaker (2021) also optimized aileron design to minimize the induced drag occurring during roll maneuvering.

Cite this article as: (2026) Suprianto A., Santoso D., Wibowo S. S., Krisbudiman, A., Dahsyat M., Gumilang R. L., Triputra F. R., Maulana J., Mukti, S. "Aerodynamic Design and CFD-based Performance Analysis of UAV Wing Ailerons", Periodica Polytechnica Transportation Engineering, https://doi.org/10.3311/PPtr.41231

Designing and testing drones is important for improving how they fly and solving problems. Studies show that using drones for deliveries and in air traffic is getting more complex. Sándor, (2023a) pointed out issues like infrastructure and rules that delivery drones face, highlighting the need for good design to make them work well. In another study, Sándor (2023b) looked at the challenges of controlling drones, emphasizing the need for well-designed parts like ailerons to keep them stable. Jiang et al. (2025) suggested a model for city drone airports and routes, noting that design affects energy use and delivery distances. New materials in drone building need careful testing. Kierzkowski et al. (2024) showed that how fibers are arranged in materials affects their properties, stressing the need to consider this in tests. Safety systems have also improved. Tomiło (2025) introduced a system using AI to help pilots spot other aircraft and avoid crashes, improving stability. These studies show that good design, strong materials, and smart systems are key for safe and efficient drone use.

Another study employs numerical methods to evaluate and optimize the aerodynamic design of the aileron based on computational fluid dynamics (CFD). Using CFD, detailed analyses of airflow, pressure distribution, and control moment effectiveness can be conducted, enabling the optimization of aileron geometry to enhance aerodynamic efficiency and the overall performance of unmanned aerial vehicles. Besides that, the study utilizes advanced numerical methods centered on computational fluid dynamics (CFD) to rigorously evaluate and optimize the aerodynamic design of the aileron. By simulating airflow patterns and pressure distributions around the control surface, CFD enables a detailed understanding of the complex fluid-structure interactions that influence control effectiveness and aerodynamic forces. This approach allows researchers to identify critical design parameters and iteratively refine the aileron geometry, ensuring improved lift-to-drag ratios and enhanced stability during various flight conditions.

Through these simulations, the control moment generated by the aileron can be quantified, assessing how modifications to shape, size, and deflection angles impact maneuverability and overall aircraft performance. The optimization process driven by CFD results in an aileron design that not only maximizes aerodynamic efficiency but also contributes to the operational reliability and responsiveness of unmanned aerial vehicles (UAVs). This methodical, data-driven design refinement is essential for advancing UAV capabilities in terms of speed, agility, and energy efficiency (Herdiana et al., 2024; Suprianto et al., 2024; Rahmah et al., 2020; Pavlenko and Pigusov, 2018).

2 Setup and methodology

2.1 The concept of control surface design

In the field of flight control, the primary function is to generate force moments, which are determined by the design of aircraft control surfaces. Specifically, the selection of control surface configurations involves several critical considerations. And it is supported by several iterations to produce the optimal design in meeting the specified safety factors and technical specifications (Krisbudiman et al., 2024). Ultimately, the configuration of control surfaces directly influences the aircraft's performance, safety, and overall operational efficacy as outlined below:

a. The function of control surfaces
   The primary control surfaces (elevator, aileron, rudder) are utilized to regulate the aircraft's movement along its three principal axes: roll, pitch, and yaw. The design of control surfaces with coupled roll-yaw moment not only impacts stability and maneuvering but also plays a crucial role in optimizing aerodynamic performance and structural efficiency (Brincklow and Hunsacker, 2021).
b. Configuration of control surfaces
   The general classification of various configurations commonly used in designing aircraft control surfaces includes ailerons, rudder, elevator, all-moving horizontal tail, taileron, elevon, and ruddervator. This research focuses on the primary design of the aileron to address the stability of roll and yaw motions (Sadraey, 2012); (Mavris and Pinon, 2012).
c. The influence of aircraft class on control surface design
   Aircraft are categorized into four classes (I-IV) based on maximum takeoff weight (MTOW) and maneuverability (Xu and Qiu, 2010; FAA, 2018). Smaller aircraft (Class I) tend to exhibit higher maneuverability, requiring control surfaces to be more responsive (Zhang and Guo, 2025). Meanwhile, Class IV aircraft (such as aerobatic and fighter jets) demand highly precise control surfaces capable of handling substantial aerodynamic loads.
d. Handling quality and flight phases
   Each flight phase (takeoff, climb, cruise, approach, landing) requires distinct control surface functionalities. During the takeoff and climb phases, pitch stability and control are critical, while the cruise phase

demands optimal aerodynamic efficiency (Greene et al., 2014). Additionally, the approach and landing phases require precise yaw control to ensure a safe landing (Klyde et al, 2020).

Primary control surfaces like elevator, aileron, and rudder control aircraft through roll, pitch, and yaw. Their design affects stability and flight performance. Ailerons enable roll and yaw stability. Aircraft are classified by takeoff weight and maneuverability, determining control responsiveness. Different phases need specific controls: pitch for takeoff, efficiency for cruising, and yaw for landing.

During these critical phases, the aircraft's yaw control, primarily managed by the rudder, plays a pivotal role in maintaining directional stability and alignment with the runway centerline. This is particularly crucial in crosswind conditions, where the aircraft must counteract lateral forces to prevent drift and ensure a smooth touchdown (Herrington et al., 2023).

Aileron design must satisfy multiple and often competing requirements, including roll control authority, response time constraints, structural efficiency, and aerodynamic effectiveness. The design process integrates a sequence of analytical methods, beginning with the identification of design requirements and objectives, followed by the configuration of the control surface, and the establishment of maneuverability and roll control criteria based on mission specifications and aircraft classification.

Fig. 1 illustrates the determination of optimal aileron parameters, Computational Fluid Dynamics (CFD) simulations are employed to validate the aerodynamic behavior under realistic operating conditions. The final design is then analyzed to ensure compliance with the specified maneuverability requirements and to optimize performance in terms of roll responsiveness and control stability.

2.2 Empirical analysis method

The aileron control surface functions to generate rolling moments around the longitudinal axis, enabling roll control. Roll control forms the fundamental basis for aileron design. The dimensions of the aileron are typically determined based on takeoff or landing phases, where aircraft speed is at its lowest. Roll control quality requirements for aircraft with a maximum takeoff weight (MTOW) below 6,000 kg fall under Class I, with critical flight phases requiring a roll angle, (ϕ_{des}) of 30° to be achieved within 1.3 seconds at Acceptance Level 1 (Sanghi et al., 2024; Sanghi et al., 2023; Healy et al., 2021).

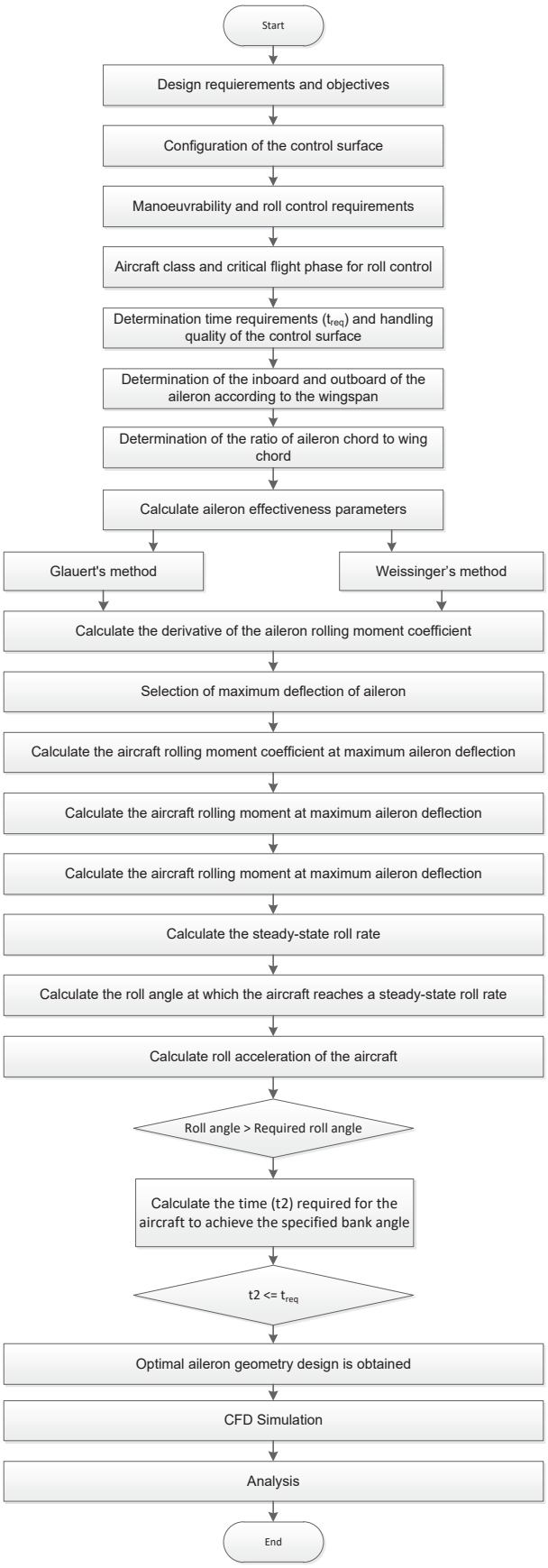

Fig. 1 Flowchart of aileron parameter optimization (Hewson, 2018)

The initial design positions for the inboard and outboard locations were selected at 75% and 95% of the wingspan, respectively. The rear spar of the wing is located at 75% of the wing chord, leaving 25% of the area available for the aileron. The chord ratio of the aileron to the wing chord was determined accordingly c_f/c amounting to 20%. The effectiveness parameter of the aileron τ_a is determined using Eq. (1) which is the original Glauert method (Glauert, 1927) or Eq. (2) which is derived using the Weissinger-Wieghart Method.

$$\tau_a = 1 - \frac{\phi + sin\phi}{\pi} \tag{1}$$

Eq. (2) was derived by the author as part of the development of a previous empirical method, contributing to the novelty of this research. This derivation was inspired by the formulation mentioned by McCormick in flight (Nangia, 1996; Raol and Singh, 2023) regarding effectiveness, which was obtained using Weissinger's method based on the work of Weissinger, (1947). Weissinger referred to this approach as "The Lifting-Line Method (L-Method)". According to Weissinger, (1947), this approach was first introduced by Wieghardt (1939). Therefore, the author refers to this approach as the Weissinger-Wieghart method. This novelty lies in its ability to define a quantitative lower bound of aileron effectiveness using a hybrid analytical-empirical framework that avoids the computational overhead associated with high-fidelity CFD or flight simulation models.

The Weissinger-Wieghart approach is based on the results of symmetric airfoil analysis using thin airfoil theory and the Kutta-Joukowski theorem, which states that lift force is equal to the product of flow density, circulation, and free-stream velocity (Taha and Gonzalez, 2023).

This derivation begins by modeling the airfoil as two sequential flat plate segments (sections, panels): one flat plate with a length of $x_f = c - c_f$ and another with a length of c_f acting as a flap. By deflecting this "flap" we can observe its influence on the lift coefficient. The approach is illustrated in Fig. 2, which presents the schematic application of the Weissinger method using the two-panel approach (2-panel method) to analyze the aerodynamic behavior of an airfoil equipped with a flap.

This method is a simplification of the vortex lattice method, which is used to analyze the circulation distribution along the airfoil chord and account for the effect of flap deflection on the lift force distribution. This can be described for each panel according to the definition of

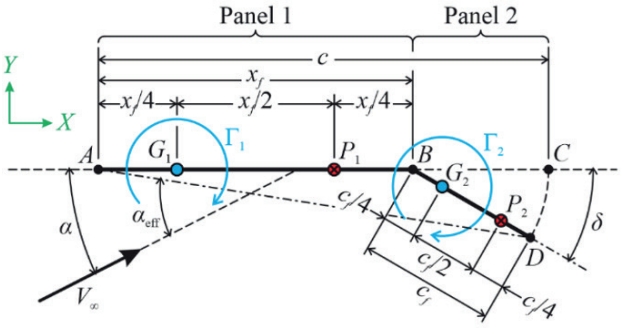

Fig. 2 Application of the Weissinger Two-Panel Method for a Flapped Airfoil (Nangia, 1996)

the Cartesian coordinate axes, where the *X*-axis is parallel to the airfoil chord and the *Y*-axis is perpendicular to the flat plane. The panel in the first segment corresponds to section *AB*, while the second segment corresponds to *BD* (which, in its initial state, is).

Next, G_1 and G_2 represent the locations of the bound vortices, while P_1 and P_2 are the control points, which are sequentially placed at $c/4$ and $3c/4$ from the leading edge of each panel, respectively. Two primary circulations, Γ_1 and Γ_2, are generated on panels 1 and 2, respectively. Weissinger's method states that the induced velocity at each control point is calculated based on the influence of other vortices using the Biot–Savart law (Liang et al., 2013). Additionally, the local angle of attack including the effects of flap deflection is used to determine the lift distribution.

The result of this study on the Weissinger-Wieghart method is the following Eq. (2).

$$\tau_a = \frac{3\left(3 - 2\frac{c_f}{c}\right)\frac{c_f}{c}}{4\left(1 - \frac{c_f}{c}\right)\frac{c_f}{c} + 3} = \frac{3\frac{c_f}{c}}{1 + 2\frac{c_f}{c}}, \tag{2}$$

Using Eq. (1) and (2), the results can be processed as presented in Fig. 3, where the required flap effectiveness factor τ_f based on the initial design of the available control surface aileron configuration according to calculations from the Glauert equation approach and the Weissinger-Wieghart method ranges between 0.45 and 0.55. This dimensionless parameter is expected to quantify how effectively aileron deflection contributes to lift (or moment) variation on the airfoil.

After obtaining the aileron effectiveness value, the next step is to calculate the rolling moment coefficient of the aileron ($C_{\ell_{\delta_a}}$) using the following equation:

$$C_{\ell_{\delta_a}} = \frac{2C_{L_{\alpha_w}}\tau_a c_r}{Sb}\left[\frac{y^2}{2} + \frac{2}{3}\left(\frac{\lambda - 1}{b}\right)y^3\right]_{y_i}^{y_o}. \tag{3}$$

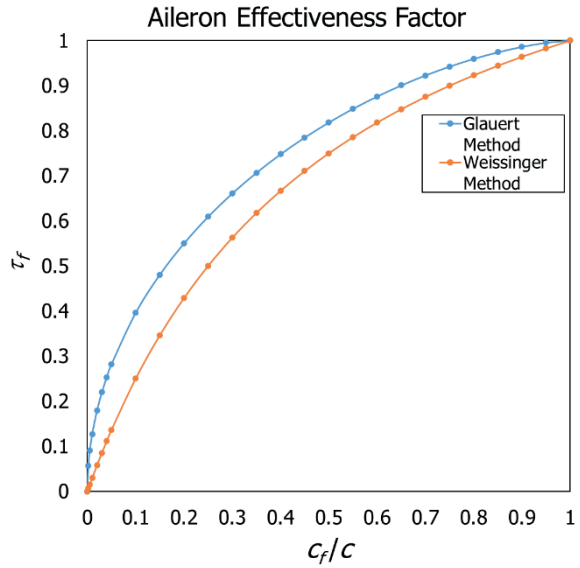

Fig. 3 Control surface effectiveness factor

The next step involves calculating the aircraft's rolling moment coefficient (C_ℓ) at the maximum aileron deflection angle ($\delta_{a_{\max}}$) using the designated equation. The aileron deflection angle is selected to be ±20 degrees (Sadraey, 2012).

$$C_\ell = C_{\ell_{\delta_a}} \delta_{a_{\max}} \tag{4}$$

The rolling moment of the aircraft (M_x) corresponds to the lift force generated when the aileron is deflected at its maximum angle, and it is calculated using the following equation:

$$M_x = \mathcal{L} = \frac{1}{2} \rho V_{\text{app}}^2 S b C_\ell \,. \tag{5}$$

Approach speed (V_{app}) is generally 1.1–1.3 times the stall speed (Gudmundsson, 2013). As a result, the aircraft is considered to approach the runway at a speed of 1.3 . Additionally, sea level altitude is taken into account for landing flight operations.

Rate of steady rolling moment motion (p_{ss}) is calculated using Eq. (6) below, the rolling drag force coefficient is determined (C_{D_R}) on a wing with the value of 0.9, the drag moment arm (y_D) is assumed to be located at 40% of the wingspan.

$$p_{ss} = \sqrt{\frac{2\mathcal{L}}{\rho S_{\text{tot}} C_{D_R} y_D^3}} \tag{6}$$

Bank angle (ϕ_1): Where the aircraft achieves a steady roll rate, it is calculated using the following equation:

$$\phi_1 = \frac{I_{xx}}{\rho S_{\text{tot}} C_{D_R} y_D^3} \ln\left(p_{ss}^2\right). \tag{7}$$

The speed of roll rate (rate of roll-rate), or the roll acceleration of the aircraft (roll acceleration), ($\dot{p}$), generated by the rolling moment of the aileron, the aircraft's steady-state roll rate (p_{ss}), is calculated using the following equation:

$$\dot{p} = \frac{p_{ss}^2}{2\phi_1} \,. \tag{8}$$

The next step is to calculate the time (t_2) required for the aircraft to achieve the specified bank angle, (ϕ_{des}) using the given equation:

$$t_2 = \sqrt{\frac{2\phi_{\text{des}}}{\dot{p}}} \,. \tag{9}$$

The roll moment acceleration requirement, expressed mathematically as a function of time (t_2), plays a crucial role and is highly dependent on the dimensions of the designed aileron control surface configuration. If the obtained duration is shorter than the required time, the solution is to increase the size of the aileron (span or chord length) or to enhance the maximum aileron deflection. However, due to stall issues on the aileron and the location of the rear spar, the maximum aileron deflection and the chord-to-wing ratio remain unchanged. By plotting the roll angle (ϕ_{des}) against time (t_2) based on Eq. (9), an exponential mathematical relationship is obtained, as shown in Fig. 4. This curve illustrates the minimum required roll angle limit up to the prescribed threshold, as previously explained.

2.3 Computational analysis method

In the CFD simulation, the turbulence model utilized is the SST (Shear Stress Transport) combining with model, as it is necessary to account for the accuracy pressure gradient along the wing surface (Badran et al., 2025). The pressure

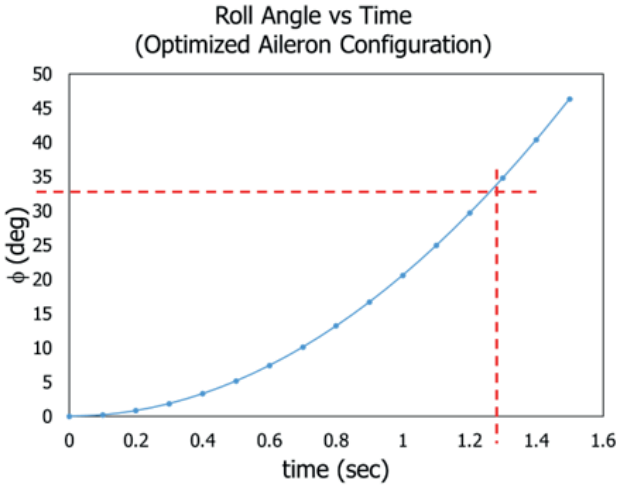

Fig. 4 Roll angle vs time (Optimized aileron configuration)

variations occurring in the fluid flow over distance create a pressure gradient that significantly impacts the behavior of the boundary layer—a thin fluid layer adjacent to the surface of an object moving relative to the fluid flow (Adeel-Ur-Rehman et al., 2024; Liang, 2020; Matyushenko and Garbaruk, 2016). The effects of pressure gradients on the boundary layer influence various phenomena, such as the development of flow separation (Prakash et al., 2024; Balin and Jansen, 2021). The effects of pressure gradients on the boundary layer can be analyzed using the Boundary Layer Equation, which is a simplified form of the Navier-Stokes equations. This equation is expressed as:

$$\frac{\partial u}{\partial t}+u\frac{\partial u}{\partial x}+v\frac{\partial u}{\partial y}=\frac{-1}{\rho}\frac{\partial p}{\partial x}+v\frac{\left(\partial^2 u\right)}{\left(\partial y^2\right)}. \tag{10}$$

Where u and v are the velocity components, with u representing the flow direction parallel to the main flow and v perpendicular to it, while $\partial p/\partial x$ represents the pressure gradient along the main flow direction within the fluid's kinematic viscosity v.

The SST model interprets turbulence using the k-ω formulation near the wall and the k-ε formulation in regions of flow farther from the wall. This turbulence model is composed of two transport equations: one for k, representing turbulent kinetic energy, and another for ω, representing specific dissipation rate (Mishra et al., 2021), each with their respective definitions as follow:

$$\frac{\partial\left(\rho k\right)}{\partial t}+\frac{\partial\left(\rho u_i k\right)}{\left(\partial x_i\right)}=P_k-\rho\beta^*\omega k + \frac{\partial}{\left(\partial x_i\right)}\left[\left(\mu+\sigma_k\mu_t\right)\frac{\partial k}{\left(\partial x_i\right)}\right], \tag{11}$$

$$\frac{\partial\left(\rho\omega\right)}{\partial t}+\frac{\partial\left(\rho u_i\omega\right)}{\left(\partial x_i\right)}=\frac{\gamma}{v_t}P_k-\rho\beta\omega^2 + \frac{\partial}{\left(\partial x_i\right)}\left[\left(\mu+\sigma_\omega\mu_t\right)\frac{\partial\omega}{\left(\partial x_i\right)}\right]+2\left(1-F_1\right). \tag{12}$$

2.4 Parameter setup

The focus of this design study is to determine the size and position of the ailerons that meet the criteria of military standards MIL-STD-1797 (Takahashi et al., 2025). As an initial guideline, the inner edge of the aileron is positioned at 60% of the wingspan on either the right or left wing, while the outer edge is positioned at 95% of the wingspan on either side. Additionally, it is assumed that the UAV is equipped with two spars (wing beams), located at the front and rear sections of the inner wing. The front and rear spar are positioned at ¼ c and ¾ c.

Fig. 5 illustrates the top view of the unmanned aerial vehicle (UAV), complete with its main dimensions and control surface configuration, particularly the ailerons, using a coordinate axis system X_d, Y_d, and Z_d as a frame coordinate. Using a scale of 1:80 in millimeters, the UAV's key dimensions include an overall length of 17,000 mm and a fuselage width at the wing root (body width) of approximately 1,210 mm. The dimensions and wing configuration feature a root wing chord (c_r) at the center, with a length of 1,210 mm. Applying a linear equation, the chord along the wingspan, $c(y)$ forms a tapered planform, meaning that as the wing extends outward, the chord length gradually decreases.

The aileron area is marked on the outer section of the wing (highlighted in red), with details indicating the width of the aileron tip area, (c_{F0}), positioned relative to the wing's tip chord (c_{tip}) at 490 mm. Meanwhile, the width of the aileron's root area, (C_{FI}), is measured from the difference

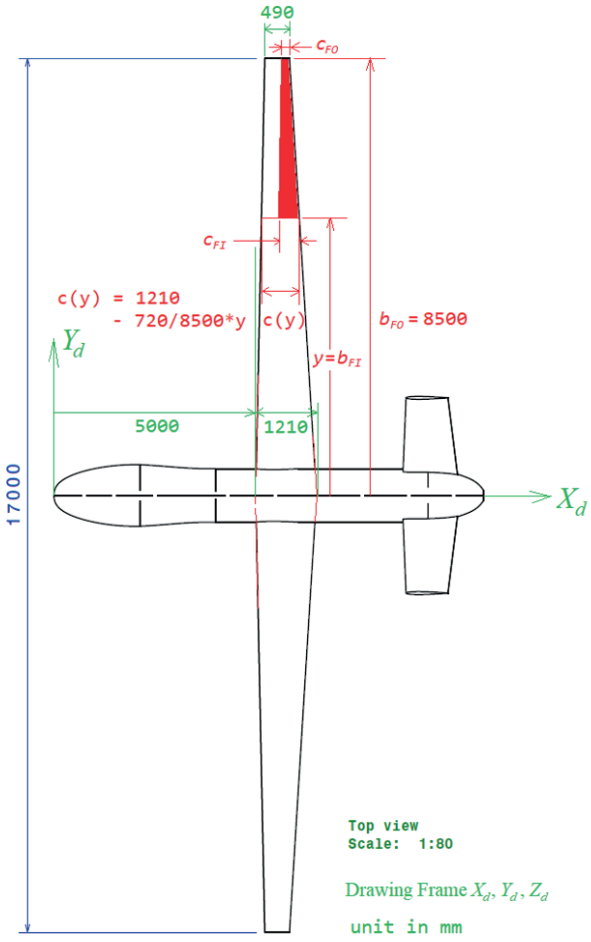

Fig. 5 UAV aileron configuration model

between the root chord and $c(y)$. Furthermore, the length of the aileron is calculated as the difference between the total half span of the wing, (b_{F0}), which is 8,500 mm, and the length $y = b_{FI}$ from the fuselage centerline, where the wing's distance to the datum is approximately 5,000 mm.

The design and characteristics of the aileron, located on the outer section of the wing with a tapered model starting from the mid-span and extending towards the wingtip, are highly effective. This configuration generates a large roll moment with a significant moment arm while simultaneously enhancing the roll maneuver responsiveness to improve maneuverability and precision, which is particularly advantageous for tasks requiring agility, such as surveillance of the UAV (Sanghi et al., 2020).

The unmanned aerial vehicle (UAV) utilized in this study was configured with a set of baseline parameters that were carefully selected to optimize aerodynamic performance while ensuring stability and controllability during various phases of flight. The key configuration data of the UAV are summarized in Table 1. The UAV features a mean take-off weight, (m_{T0}) of 1,300 kg, categorizing it into the medium-altitude, long-endurance (MALE) class of UAVs. The main wing spans a total length, (b) of 17,000 mm, combining lightweight structural design with a high aspect ratio to achieve efficient aerodynamic performance. The wing adopts a tapered planform with a root chord, (c_r) of 1,210 mm and a tip chord, (c_t) of 490 mm, resulting in a taper ratio, (λ) of 0.405. This configuration is known to effectively reduce induced drag while maintaining satisfactory structural efficiency.

The wing planform area, (S_w) is 14.45 m², supporting a relatively high wing aspect ratio, (A_R) of 20. Such a high aspect ratio is typical for UAVs intended for long-endurance missions, as it enhances the lift-to-drag ratio critical for prolonged loitering operations. Complementing the main wing, the tail or horizontal stabilizer has a planform area, (S_{hv}) of 3.803 m². The configuration ensures sufficient stability margins for various maneuvers and environmental conditions encountered during typical mission profiles. From an aerodynamic performance perspective, the wing achieves a maximum lift coefficient, ($C_{L\max}$) of 1.65, supporting a stall speed, (V_s) of 29.551 m/s. This relatively low stall speed facilitates safer take-offs and landings, particularly in confined or rugged operational environments.

Table 1 UAV wing configuration and baseline data

Parameters	Symbol	Value	Unit
Mean Take-off Weight	m_{T0}	1,300	kg
Main Wingspans	b_w	17	m
Wing Root Chord	c_r	1.21	m
Wing Tip Chord	c_t	0.49	m
Wing Taper Ratio	λ	0.405	[-]
Wing Planform Area	S_w	14.45	m²
Wing Aspect Ratio	A_R	20	[-]
Max Lift Coefficient	$C_{L\max}$	1.65	m²
Stall Speed	V_s	29.551	m/s
Wing Lift Curve Slope	$C_{L\alpha.w}$	6.1	1/rad
Inertia Moment about Longitudinal Axis	I_{xx}	5,870.31	kg·m²

Additionally, the wing lift curve slope, ($C_{L_{\alpha_w}}$) is measured at 6.1 per radian, indicating strong lift generation capability with changes in angle of attack, critical for effective pitch control. The UAV's longitudinal dynamics are further characterized by a moment of inertia about the longitudinal axis, (I_{xx}) of 5,870.31 kg·m², ensuring adequate roll stability while preserving roll maneuverability.

In the calculation of the control surface configuration dimensions for the designed aileron, based on the numerical empirical method, Eq. (13) to (15) are utilized. Specifically, Eq. (13) is used to determine the control surface span length, with the outboard and inboard position limitations represented sequentially by u% and z%, which are adjusted according to the semi-span wing dimensions, (b_w/2).

$$\bar{b}_a = \bar{b}_{a_{outboard}} - \bar{b}_{a_{inboard}}, \tag{13}$$

Where,

$$b_{a_{outboard}} = y_O = u\%(b_W / 2)$$
$$b_{a_{inboard}} = y_i = z\%(b_W / 2)$$

Next, the chord length of the control surface is calculated based on Eq. (14), considering the positional percentage (v%) relative to the chord width dimension of the wing semi-span at both the outboard and inboard positions.

$$\begin{aligned} c_{a_{inboard}} &= v\% c_{w_{inboard}} \\ c_{a_{outboard}} &= v\% c_{w_{outboard}} \end{aligned} \tag{14}$$

Where,

$$c_{w_{inboard}} = c_r \left[1 + 2\left(\frac{\lambda - 1}{b_w} \right) y_i \right]$$

$$c_{w_{outboard}} = c_r \left[1 + 2\left(\frac{\lambda - 1}{b_w} \right) y_O \right]$$

The values for the wing root chord (c_r), wing taper ratio (λ), and main wing span (b_w) can be found in Table 1.

The control surface area (S_a) is calculated based on the complete set of obtained parameter data for a single cross-sectional area of the wing semi-span, using Eq. (15), which represents the equation for the area of a trapezoidal flat surface.

$$S_a = \left[\frac{ca_{inboard} + ca_{outboard}}{2} \right] \bar{b}_a \tag{15}$$

The dimensional configuration of the aileron control surface will be optimized based on considerations for the structural layout composition of the wing, which is constructed with two spars: the main spar and the rear spar. This aspect is crucial in terms of elasticity constraints, given the considerable overall wingspan.

The numerical simulation process begins with the geometry of the airfoil, derived from the cross-sectional profile of the UAV wing model as shown in Fig. 6. This profile is taken from the middle section of the aileron-wing, positioned at the trailing edge of the wing and near the wingtip, in line with the typical configuration of lateral control systems. The cross-sectional results of the aileron on one wing can be displayed at deflection angles of 0 degrees and 45 degrees. For the inner aileron section without deflection, the total chord length of the airfoil measures 602.76 mm, while the aileron chord length is 98.62 mm, approximately 16.37% of the total chord length.

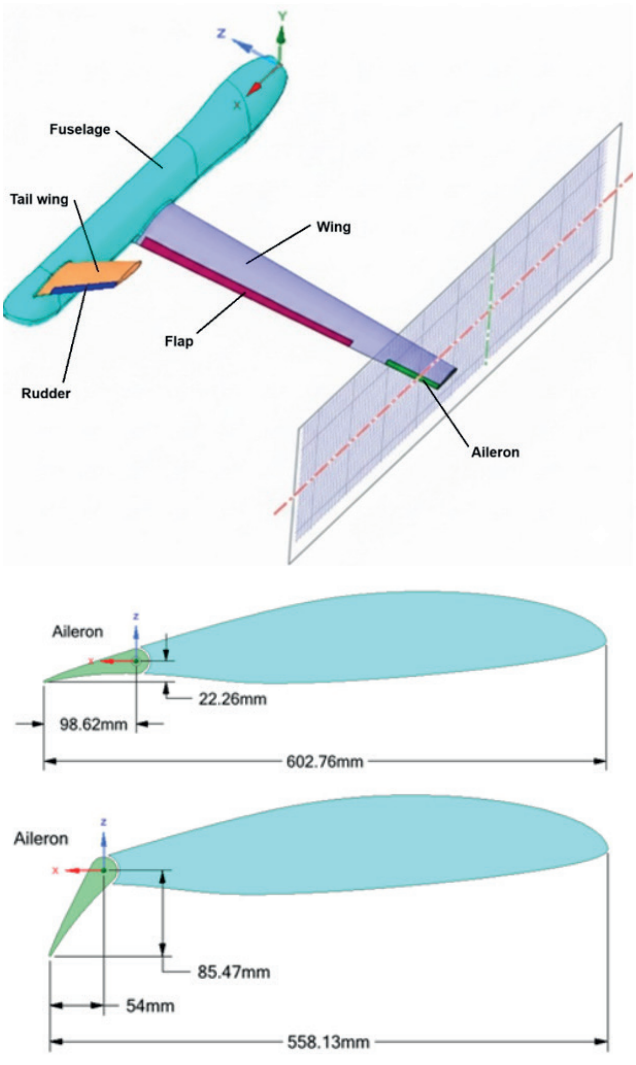

Fig. 6 The cross-sectional view of the midsection of the aileron at 0° and 45° deflection on the UAV wing model

Next, the offset height of the aileron from the airfoil axis (Z-direction) is 22.26 mm. With a deflection angle of 45 degrees, where the aileron is positioned at the trailing edge and uses a local rotation axis based on the x-z axis, the total airfoil chord length is approximately 558.13 mm, while the aileron chord length becomes 54 mm. The offset height of the aileron from the surface is 85.47 mm. It is observed that the relative size of the aileron compared to the airfoil decreases as it moves farther from the root to the tip, adhering to the principles of tapered wing control surface design. This reduces wingtip loading and enhances aerodynamic efficiency.

The key aspects considered in the setup of the CFD simulation are related to the properties of the working fluid, namely air flowing at a velocity of 37 m/s. The boundary condition at the velocity inlet in front of the wing corresponds to a Reynolds number of approximately 2.4×10^6 under sea-level conditions, with an operational pressure environment of 1.01×10^5 Pa. This external subsonic flow is classified as an incompressible flow, with a constant air density of 1.225 kg/m^3 and a viscosity of 1.79×10^{-5} kg/m.s. The turbulent flow passing through the wing airfoil employs the SST k-omega viscous model, which is recommended for aeronautical applications, with a turbulence viscosity ratio of 10. Finally, the boundary condition at the trailing edge of the wing is set as a pressure outlet with a gauge pressure of 0 Pa (Péter and Lakatos, 2023).

On the surface of the wing airfoil and the aileron control surface, a boundary condition is applied consisting of a stationary wall and a no-slip fluid condition (airflow velocity on the airfoil surface is 0 m/s). Additionally, the wall is assumed to have a smooth surface with a roughness constant of 0.5.

The mesh convergence study from Table 2 was conducted to ensure that the simulation results (aerodynamic force coefficients) are not significantly affected by the number of mesh elements but have stabilized with changes in mesh size. This is crucial to guaranteeing accuracy while avoiding the unnecessary use of computational resources.

Table 2 Mesh independence study for 2D airfoil wing aileron

Mesh Level	No. of Elements	Cell Size (near wall)	$\Delta\%\ C_l$	$\Delta\%\ C_d$
Coarse	55,876	0.0075	8.4%	11.7%
Medium	374,824	0.0045	2.1%	4.3%
Fine	776,654	0.00125	0.7%	1.3%

With mesh results consistently aligned with convergence values, the variations in lift coefficient, (C_l) and drag coefficient, (C_d) averages between the medium and fine meshes are minimal (±1%), indicating that the results have achieved mesh convergence. However, significant differences are observed between the coarse and medium meshes, demonstrating that the coarse mesh lacks sufficient accuracy. Meanwhile, the moment coefficient, c_m remains relatively stable, reflecting the consistency of simulation outcomes across different mesh resolutions. The findings are illustrated in Fig. 7.

3 Result and analysis

Fig. 8 presents a detailed top-view design layout result of the right wing geometry, illustrating key structural and aerodynamic features essential for control surface integration. The wing exhibits a classic tapered planform, with a root chord of 1.21 m and a tip chord of 0.49 m, yielding a taper ratio of approximately 0.405. Such a configuration is typically adopted to reduce induced drag while optimizing structural weight and aerodynamic performance. By maximizing the configuration of the existing wing dimensions, the control surface design process for determining the aileron length ($\bar{b}_a$) is constrained to approximately 68.9% of the wing semi-span (b_w), which is 8.5 m for the inboard wing position (y_i) with a value of approximately 5.8565 m, and 95% for the outboard wing position (y_o) or 8.0750 m. As a result, the optimal aileron control surface length is determined to be 2.2185 m.

Besides that, chordwise, the aileron is positioned aft of the rear spar located at 75% of the local chord, which aligns with standard practice in control surface design to ensure sufficient moment arm and structural support. This positioning ensures that deflection of the aileron induces an efficient rolling moment without compromising wing integrity. The aileron chord dimension is determined to be 20% of the chord length of the wing semi-span. Specifically, for the inboard section, which measures 0.7139 m, the corresponding aileron chord length is 0.1428 m, while for the outboard section, which measures 0.5260 m, the aileron chord length is 0.1052 m.

To evaluate the aerodynamic influence of aileron deflection on a UAV wing section, a computational fluid dynamics (CFD) simulation was conducted under steady-state conditions with a uniform freestream velocity of 37 m/s. Two configurations were analyzed: aileron deflected at 0° (neutral) and 45° (maximum downward deflection). The simulations provided detailed insights into the flow field behavior, specifically through the examination of velocity contours, and pressure distributions, vorticity fields, and streamlines around the airfoil with the respective aileron angles.

Fig. 9 displays the velocity contour distributions around the airfoil section for both aileron deflection angles. At 0° deflection, the flow remains mostly attached along the upper surface of the airfoil, with smooth streamlines and a well-defined velocity gradient. The high-speed region appears symmetrically distributed along the upper camber line, with a peak velocity reaching approximately 76 m/s

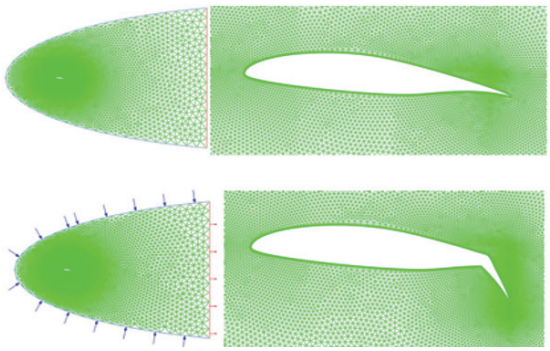

Fig. 7 Convergent mesh result for wing airfoil of aileron deflection 0° and 45°

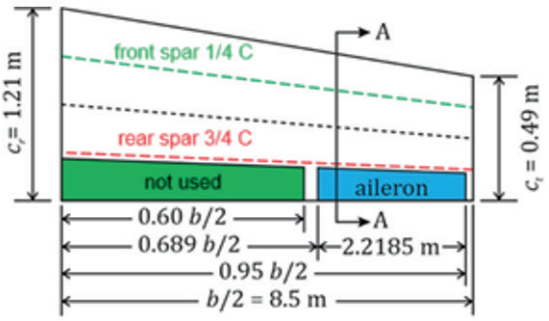

Fig. 8 Right wing top view

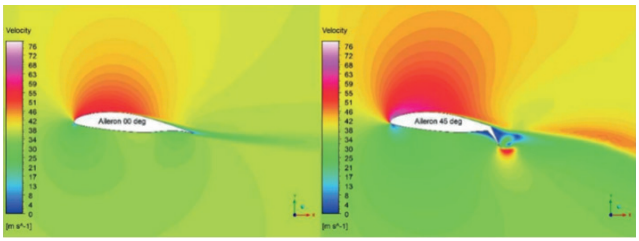

Fig. 9 Velocity contours of wing aileron deflection -0° and 45°

near the leading edge suction peak. In contrast, at a 45° downward deflection, a significant alteration in the flow field is observed. The deflected aileron causes local flow separation near the trailing edge, evident from the recirculation region and the formation of a wake vortex. This separation induces a localized velocity drop near the lower surface with value of 4 m/s until 13 m/s, and a high-velocity jet flow with 63 m/s on the upper surface downstream of the aileron hinge line. The asymmetric flow structure at 45° deflection introduces a pronounced rolling moment, essential for control surface authority.

Fig. 10 illustrates the absolute pressure distribution for both deflection angles. At 0°, the pressure field maintains a typical airfoil behavior, with lower pressure on the upper surface and higher pressure on the lower surface at difference value from about 100.757 Pa to 101.632 Pa with 102.07 Pa of stagnation pressure point, enabling efficient lift generation. The pressure difference remains modest and smoothly distributed. With aileron deflected downward at 45°, the pressure distribution changes dramatically. A strong low-pressure region forms on the upper surface just upstream of the aileron hinge, while the pressure on the lower surface significantly increases near the deflected trailing edge. This creates a steep pressure gradient from 99.225 Pa to 102.07 Pa, further confirming the generation of additional rolling moment. Furthermore, a distinct low-pressure wake region develops downstream at 99.006 Pa, indicative of increased aerodynamic drag and potential flow unsteadiness due to vortex shedding.

As shown in Fig. 11, the baseline case with 0° deflection demonstrates a smooth, symmetric flow distribution over the airfoil. The highest velocity region is concentrated over the upper surface, indicating effective lift generation with minimal flow separation. The 45° deflection case introduces substantial streamline distortion. A clear separation zone is visible near the trailing edge of the deflected aileron, forming a recirculation bubble and inducing a broader wake region. Streamlines are deflected sharply downward as they encounter the altered surface contour, leading to reversed flow near the lower surface just behind the hinge.

The vorticity contour plots distribution of rotational flow intensity are shown in Fig. 12. For the wing aileron deflection of 0°, the flow remains largely attached to the airfoil surface between at 13/s and 15/s, and the vorticity is concentrated in a narrow shear layer near the trailing edge, suggesting laminar-to-transitional boundary layer behavior without significant separation. When this part is deflected

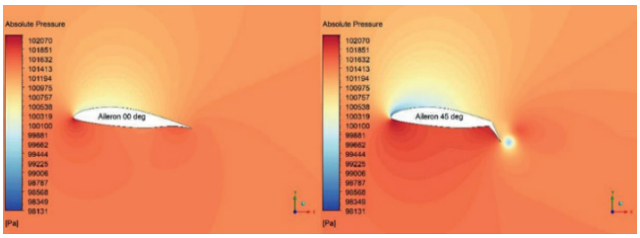

Fig. 10 Pressure contours of wing aileron deflection -0° and 45°

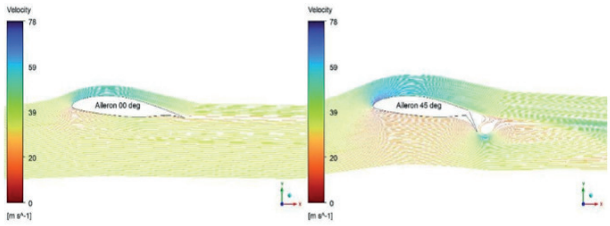

Fig. 11 Velocity streamlines of wing aileron deflection- 0° and 45°

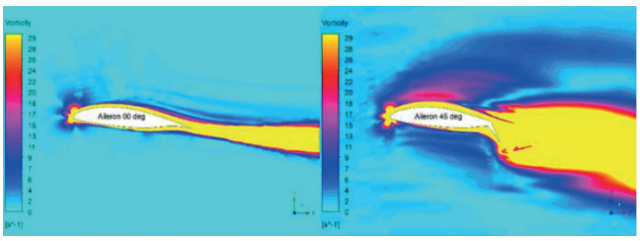

Fig. 12 Vorticity contours of wing aileron deflection -0° and 45°

to 45°, a dramatic change is observed in the wake region. High-intensity value vorticity regions with 29/s appear near the hinge point and extend downstream, forming complex vortex structures far from deformation airflow.

This indicates that the deflected aileron introduces a strong adverse pressure gradient, triggering local flow separation and vortex shedding. The peak vorticity values increase significantly, especially along the suction side and downstream of the trailing edge, highlighting the development of unsteady aerodynamic phenomena such as flow instability and potential buffeting.

The symmetric vorticity distribution in the 0° configuration supports steady aerodynamic behavior, while the asymmetry and increased vortex activity in the 45° case point to enhanced aerodynamic drag and possible reduction in control surface effectiveness due to separated flow.

Table 3 presents a comparative summary of the aerodynamic coefficients and force responses for two different aileron deflection angles: 0° (baseline condition) and 45° (maximum deflection). The variations in lift coefficient, (C_l), drag coefficient, (C_d), aerodynamic forces, and hinge moment demonstrate the aerodynamic consequences of control surface deflection.

Table 3 Results of the CFD Simulation

No	Parameter	C_l	C_d	Drag Force (N)	Lift Force (N)	Hinge Moment (Nm)
1	Aileron deflection 0 degree	0.04657	0.00712	43.16	282.12	14.8389
2	Aileron deflection 45 degree	0.06456	0.10063	609.64	391.10	59.07

When the aileron is in the neutral position of 0°, the lift coefficient, (C_l) is recorded at 0.04657, generating a lift force of 282.12 N, while the drag coefficient, (C_d) is relatively low at 0.00712, resulting in a drag force of only 43.16 N. This reflects an efficient flow condition with minimal aerodynamic penalties and low control load requirements, as indicated by the moderate hinge moment of 14.84 Nm.

However, under aileron deflection of 45°, a significant change in aerodynamic performance is observed. The lift coefficient, (C_l) increases to 0.06456, corresponding to a lift force of 391.10 N, a 38.6% increase compared to the 0° configuration. This rise in lift is attributed to the altered flow pattern induced by the aileron deflection, which effectively increases the camber on the affected side of the airfoil.

Nonetheless, this improvement in lift comes at a considerable aerodynamic cost. The drag coefficient, (C_d) experiences a sharp increase to 0.10063, and the associated drag force escalates to 609.64 N, representing more than a 1.3% increase from the baseline condition. This substantial drag penalty indicates flow separation and increased pressure drag as supported by the earlier vorticity and streamline contour analysis. To further assess the aerodynamic efficiency of the control surface deflections, the Lift-to-Drag Ratio (L/D) is evaluated for each aileron deflection case. The L/D ratio serves as a critical parameter in determining the aerodynamic performance of an airfoil, particularly in balancing lift generation against parasitic and pressure drag penalties. From the simulation results, -with calculating lift force divided by drag force of the airfoil at aileron deflection of 0° and 45° the results are 6.54 and 0.64, respectively. Despite the increased lift force, the drag escalates disproportionately, severely compromising the overall aerodynamic efficiency. The sharp reduction in L/D ratio – nearly a 90% decrease from the neutral position – suggests the onset of large-scale flow separation, vortex shedding, and increased turbulence in the wake, as previously evidenced in the vorticity contour (Fig. 12), and velocity streamline plots (Fig. 11).

Furthermore, the hinge moment increases significantly to 59.07 Nm, approximately 4 times higher than in the 0° deflection case. This suggests a much greater mechanical load on the actuation system, which must be taken into account in the design of the control mechanism. The increased hinge moment is a direct consequence of the elevated aerodynamic forces acting on the control surface and their shifted center of pressure due to flow separation.

4 Conclusion

This study has presented a comprehensive analytical-empirical approach for the design evaluation of aileron control surfaces on a UAV, a platform classified under General Aviation (GA). The methodology focused on the aircraft's performance under landing flight conditions, which represent a critical operational regime characterized by reduced aerodynamic energy and heightened control sensitivity. Within this context, the analysis was benchmarked against military standard roll performance criteria (MIL-STD-1797), providing a robust and industry-relevant framework for assessment (Takahashi et al., 2025).

The results indicate that the minimum aileron configuration capable of meeting the MIL-STD-1797 requirements for roll maneuverability includes a maximum deflection angle ($\delta a_{\max}$) of about , a chord ratio (c_a/c_w) of 20%, and an effective spanwise length of 2.2185 meters per aileron, spanning from 68.9% to 95% of the semi-span (Takahashi et al., 2025). These values delineate the threshold of control surface geometry necessary to achieve compliant roll authority. Notably, the study establishes that any incremental increase in these design parameters would not only satisfy but potentially exceed the required roll performance, offering valuable flexibility in control system tuning. In addition, the aileron deflection scheme is physically simulated numerically, increasing the aileron deflection to 45° induces substantial aerodynamic changes, i.e., drastic decline in L/D ratio at high deflection angle, including flow separation, pressure drop, increased vorticity, and also induce flow disturbances that lead to aerodynamic inefficiencies. These results underscore the trade-off between control authority and flow stability, which must be accounted for during control surface design and actuation range determination. After using linear interpolation to get the estimation of aileron efficiency at 200 of deflection, the value of L/D is 3.92. This point performance is important because as low efficiency at high deflection angles may demand higher power inputs to overcome drag-induced resistance, particularly in electrically actuated control systems.

This methodological innovation provides a fast, cost-effective tool for aerospace designers during early-phase aircraft development, especially for GA, light electric aircraft, and UAV configurations where weight, complexity, and control authority must be carefully balanced. The insights gained from this study can be further extended to the development of adaptive or morphing aileron technologies, where compact control surfaces must deliver high authority in constrained geometries. Future research is encouraged to integrate this approach with dynamic flight simulation and structural assessment to enable a holistic, multidisciplinary optimization of control surface design in next-generation aircraft platforms.

Acknowledgement

This research was conducted through research funding from the National Research and Innovation Agency, Indonesia with a letter from the Chairman of Research Organization for Aeronautics and Space number B-465/III.1/TK.02.00/1/2025. The authors would like to thank Bandung State Polytechnic and research members for the development of control surface flaps for unmanned aircraft. This is for their contribution in carrying out calculations and CFD simulation, analyzing data and information and using all the necessary equipment.

References

Adeel-Ur-Rehman, A., Theron, J. N., Kassem, H., Stoevesandt, B., Peinke, J. (2024) "Improved performance of k − ω SST turbulence model in predicting airfoil characteristics for a wide range of airfoil thicknesses", Journal of Physics: Conference Series, 2767(2), 022064 https://doi.org/10.1088/1742-6596/2767/2/022064

Arifin, A. Z., Subchan (2017) "Navigasi dan Kendali pada Pesawat Udara Nir Awak (Puna) untuk Menghindari Halangan" (Navigation and Control of Unmanned Aerial Vehicles (UAVs) for Obstacle Avoidance), Limits: Journal of Mathematics and Its Applications, 14(1), pp. 73–87. (in: Indonesian) https://doi.org/10.12962/limits.v14i1.2123

Balin, R., Jansen, K. E. (2021) "Direct numerical simulation of a turbulent boundary layer over a bump with strong pressure gradients", Journal of Fluid Mechanics, 918, A14 https://doi.org/10.1017/jfm.2021.312

Badran, O., Azad, Z., Virk, M., Masalha, I., Alahmar, A. (2025) "Aerodynamic Performance Evaluation of the NACA 65-421 Airfoil Using CFD and the k-ω SST Turbulence Model", In: Proceedings of the ASME 2025 Aerospace Structures, Structural Dynamics, and Materials Conference. ASME 2025 Aerospace Structures, Structural Dynamics, and Materials Conference. Houston, USA, V001T01A027. https://doi.org/10.1115/ssdm2025-157721

Brincklow, J. R., Hunsaker, D. F. (2020) "Lifting-Line Analysis of Optimum Aileron Sizing to Minimize Induced Drag During Roll", In: AIAA Scitech 2020 Forum, Orlando, USA. https://doi.org/10.2514/6.2020-0279

Brincklow, J. R., Hunsaker, D. F. (2021) "Aileron size and location to minimise induced drag during rolling-moment production at zero rolling rate", The Aeronautical Journal, 125(1287) pp. 807–829. https://doi.org/10.1017/aer.2020.139

Brincklow, J. R., Montgomery, Z. S., Hunsaker, D. F. (2024) "Controlling roll-yaw coupling with aileron and twist design", The Aeronautical Journal, 128(1327), pp. 1961–1973. https://doi.org/10.1017/aer.2024.21

Dong, M., Zhang, C., Pan, T. (2024) "Research on Airworthiness Certification and Risk Control of Minimum Unstick Speed for Civil Aircraft", Advances in Computer and Engineering Technology Research, 1(4), p. 130. https://doi.org/10.61935/acetr.4.1.2024.P130

Federal Aviation Administration (2018). "Flight Test Guide for Certification of Transport Category Airplanes", [pdf] U.S. Department of Transportation Federal Aviation Administration, Washington, DC, USA, AC No: 25-7D Available at: https://www.faa.gov/documentLibrary/media/Advisory_Circular/25-7D.pdf [Accessed: MISSING]

Greene, K. M., Kunz, D. L., Cotting, M. C. (2014) "Toward a Flying Qualities Standard for Unmanned Aircraft", In AIAA Atmospheric Flight Mechanics Conference, Atlanta, GA, USA, AIAA 2014-2194. eISBN: 978-1-62410-294-3 https://doi.org/10.2514/6.2014-2194

Gudmundsson, S. (2013) "Chapter 19 - Performance – Cruise", General Aviation Aircraft Design, Elsevier, pp. 847–894. https://doi.org/10.1016/b978-0-12-397308-5.00019-2

Glauert, H. (1927) "Theoretical relationships for an aerofoil with hinged flap", H.M. Stationery Office, London, UK, Rep. 1095. [online] Available at: https://reports.aerade.cranfield.ac.uk/handle/1826.2/1412 [Accessed: 25 January 2026]

Healy, F., Cheung, R., Neofet, T., Lowenberg, M., Rezgui, D., Cooper, J., Castrichini, A. (2021) "Folding Wingtips for Improved Roll Performance", Journal of Aircraft, 59(1), pp. 15–28. https://doi.org/10.2514/1.c036372

Herdiana, D., Pinindriya, S. T., Soemaryanto, A. R., Aribowo, A., Tresnoningrum, D., Suprianto, A. (2024) "Downwash Investigation of Horizontal Tail Plane Configuration for 19-Passenger Aircraft Based on a Wind Tunnel Test", Engineering Journal, 28(12), pp. 29–39. https://doi.org/10.4186/ej.2024.28.12.29

Herrington, S. M., Zahed, M. J. H., Fields, T. D. (2023) "Handling Qualities Assessment and Performance Evaluation for Unmanned Aerial Systems and Pilots", Unmanned Systems, 12(01), pp. 99–131. https://doi.org/10.1142/s2301385024500080

Hewson, R. (2018) "Aircraft Performance: An Engineering Approach M. H. Sadraey CRC Press, Taylor & Francis Group", The Aeronautical Journal, 122(1251), pp. 841–842. https://doi.org/10.1017/aer.2018.18

Jiang, H., Wang, J., Ren, X. (2025) "Location-Route Planning for VTOL Airport and UAV Urban Logistics Network – A Case Study of Tianjin", Promet - Traffic&Transportation, 37(2), pp. 456–476. https://doi.org/10.7307/ptt.v37i2.634

Kierzkowski, A., Kisiel, T., Milewski, M., Török, Á., Stosiak, M., Wróbel, J. (2024) "Computer-aided simulation of unmanned aerial vehicle composite structure dynamics", Transport, 39(4), pp. 302–312. https://doi.org/10.3846/transport.2024.23159

Klyde, D. H., Schulze, P. C., Mitchell, D. G., Sizoo, D., Schaller, R., Mcguire, R. (2020) "Mission Task Element Development Process: An Approach to FAA Handling Qualities Certification", In: AIAA Aviation 2020 Forum, [online event]AIAA 2020-3285. https://doi.org/10.2514/6.2020-3285

Krisbudiman, A., Rezqi, K., Gumilang, R. L., Dahsyat, M., Zenal, H., Kadir, A. M., Yulianto, E. (2024) "Structural Design Analysis Torque Links of Nose Landing Gear on Light Aircraft", International Journal on Advanced Science, Engineering and Information Technology, 14(2), pp. 507–513. https://doi.org/10.18517/ijaseit.14.2.19317

Liang, C. (2020) "Effect of Closure Coefficients of K-Ω SST Turbulence Model on Predicting Stall Characteristics of The Airfoil", Journal of Physics: Conference Series, 1600(2020), 012032. https://doi.org/10.1088/1742-6596/1600/1/012032

Liang, H., Zong, Z., Sun, L., Zou, L., Zhou, L., Zhao, Y. J., Ren, Z. R. (2013) "Generalized Weissinger's L-method for prediction of curved wings operating above a free surface in subsonic flow", Journal of Engineering Mathematics, 83(1), pp. 109–129. https://doi.org/10.1007/s10665-012-9611-8

Matyushenko, A. A., Garbaruk, A. V. (2016) "Adjustment of the k-ω SST turbulence model for prediction of airfoil characteristics near stall", Journal of Physics: Conference Series, 769 (1), 012082. https://doi.org/10.1088/1742-6596/769/1/012082

Mavris, D. N., Pinon, O. J. (2012) "A Systems Engineering Approach to Aircraft Design", In: Blockley, R., Shyy, W. (eds.) Encyclopedia of Aerospace Engineering, John Wiley & Sons. ISBN 978-0470754405 https://doi.org/10.1002/9780470686652.eae597

Mishra, A., Kumar, G., De, A. (2021) "Prediction of Separation Induced Transition on Thick Airfoil Using Nonlinear URANS Based Turbulence Model", [preprint] arXiv:2102.13277v1, 26 February 2021. https://doi.org/10.48550/arXiv.2102.13277

Nangia, R. K. (1996) "Aerodynamics, Aeronautics and Flight Mechanics – Second edition, B. W. McCormick, John Wiley & Sons", The Aeronautical Journal, 100(991), p. 36. https://doi.org/10.1017/s000192400002724x

Negahban, M. H., Bashir, M., Priolet, C., Botez, R. M. (2024) "Novel Twist Morphing Aileron and Winglet Design for UAS Control and Performance", Drones, 8(8), 392. https://doi.org/10.3390/drones8080392

Pavlenko, O. V., Pigusov, E. A. (2018) "Numerical investigation of the aerodynamic loads and hinge moments of the flap with boundary layer control", AIP Conference Proceedings 1959(1), 050024. https://doi.org/10.1063/1.5034652

Prakash, A., Balin, R., Evans, J. A., Jansen, K. E. (2024) "A streamline coordinate analysis of a turbulent boundary layer subject to pressure gradients and curvature on the windward side of a bump", Journal of Fluid Mechanics, 984, A23. https://doi.org/10.1017/jfm.2024.199

Péter, B., Lakatos, I. (2023) "Comparison of Different Turbulence Models and Wall Treatment Methods for Vehicle Aerodynamics Investigations", Periodica Polytechnica Transportation Engineering, 52(1), pp. 67–74. https://doi.org/10.3311/pptr.22671

Xu, L., Qiu, T. (2010) "Flight test on wet runway in type certification of transport category airplanes", Flight Dynamics, 6, pp. 77–79. [online] Available at: https://caod.oriprobe.com/articles/25861993/Flight_test_on_wet_runway_in_type_certification_of.htm

Rahmah, S. N., Jatisukamto, G., Sutjahjono, H. (2020) "The Influence of the Reference Area of Aileron on the N2XX Aircraft Using Computational Fluid Dynamics", Journal of Mechanical Engineering Science and Technology, 4(1), pp. 28–36. https://doi.org/10.17977/um016v4i12020p028

Raol, J. R., Singh, J. (2023) "Flight Mechanics Modeling and Analysis", [e-book] CRC Press. ISBN 9781003293514 https://doi.org/10.1201/9781003293514

Sadraey, M. H. (2012) "Aircraft Design: A Systems Engineering Approach", John Wiley & Sons. ISBN 9781119953401 https://doi.org/10.1002/9781118352700

Sanghi, D., Cesnik, C. E., Riso, C. (2023) "Roll Maneuvers of Very Flexible Aircraft with Flared Folding Wingtips", In: AIAA SCITECH 2023 Forum, National Harbor, USA, AIAA 2023-0186. https://doi.org/10.2514/6.2023-0186

Sanghi, D., Cesnik, C. E. S., Riso, C. (2024) "Roll Maneuverability of Transonic High-Aspect-Ratio-Wing Aircraft with Flared Folding Wingtips", Journal of Aircraft, 61(3), pp. 915–938. https://doi.org/10.2514/1.c037470

Sanghi, D., Riso, C., Cesnik, C., Vetrano, F. (2020) "Influence of Aileron Placement on Roll Response of High-Aspect-Ratio-Wing Aircraft", In: AIAA AVIATION 2020 FORUM, Virtual Event, AIAA 2020-2645. https://doi.org/10.2514/6.2020-2645

Sándor, Z. (2023a) "Challenges in the aviation system caused by the emergence of delivery drones", Acta Technica Jaurinensis, 16(1), pp. 1–10. https://doi.org/10.14513/actatechjaur.00684

Sándor, Z. (2023b) "Challenges of the visual line of sight operations of unmanned aerial vehicles", Acta Technica Jaurinensis, 16(4), pp. 167–173. https://doi.org/10.14513/actatechjaur.00717

Suprianto, A., Hartono, F., Herdiana, D., Tresnoningrum, D., Pramana, N. (2024) "Pusher Propeller Performance Investigation on Lightweight Medium Range UAV", Engineering Journal, 28(9), pp. 11–24. https://doi.org/10.4186/ej.2024.28.9.11

Susilo, B. T., Suwondo, E., Mulyanto, T. (2024) "Pengembangan Sistem Aileron Pesawat Terbang Berbasis Elektromekanik" (Development of an Electromechanical Airfoil System for Aircraft), Mesin, 30(1), pp. 29–38. (in Indonesian) https://doi.org/10.5614/mesin.2024.30.1.2

Taha, H. E., Gonzalez, C. (2023) "Refining Kutta's Flow over a Flat Plate: Necessary Conditions for Lift", AIAA Journal, 61(5), pp. 2060–2068. https://doi.org/10.2514/1.j062273

Takahashi, T. T., Griffin, J. A., Grandhi, R. V. (2025) "High-Speed Aircraft Stability and Control Metrics", Aerospace, 12(1), p. 12. https://doi.org/10.3390/aerospace12010012

Tomiło, P. (2025) "Aircraft Pilot Assistance System: Detection of Other Aircraft Using Artificial Neural Networks", Transport and Telecommunication Journal, 26(2), pp. 103–117. https://doi.org/10.2478/ttj-2025-0009

U.S. Department of Defense (1995) "MIL-STD-1797A: Flying Qualities of Piloted Aircraft (Notice/versions as distributed)", Washington, DC, USA. [online] Available at: https://everyspec.com/MIL-STD/MIL-STD-1700-1799/MIL-STD-1797A_NOTICE-3_39377/?utm [Accessed: 26 January 2026]

Wang, L., Zhou, T. (2025) "Research on Airworthiness Certification Regulations and Design of Flight Test Methods for the Minimum Unstick Speed of Civil Aircraft", In: Liang, G., Wu, Z. (eds) Trends in Aerospace Engineering, Springer Nature Singapore, pp. 59–64. ISBN 978-981-96-6234-0 https://doi.org/10.1007/978-981-96-6235-7_7

Weissinger, J. (1947) "The Lift Distribution of Swept-Back Wings", No. 1120. National Advisory Committee for Aeronautics, Washington. [online] Available at: https://digital.library.unt.edu/ark:/67531/metadc63857/

Wieghardt, K. (1939) "Über die Auftriebsverteilung des einfachen Rechteckflügels über die Tiefe", (On the lift distribution of the simple rectangular wing along the chord), Zeitschrift für Angewandte Mathematik und Mechanik, 19(5), pp. 257–270. [in German] https://doi.org/10.1002/zamm.19390190502

Zhang, Y., Guo, T. (2025) "Flight test study on spin characteristics of light small normal category airplanes", Journal of Physics: Conference Series, 2977, 012046. https://doi.org/10.1088/1742-6596/2977/1/012046